LA-UR-17-31200
Approved for public release; distribution is unlimited.

Title: The Role of Grain Boundary Orientation on Void Nucleation in Tantalum

Author(s): Hahn, Eric Nicholas
Fensin, Saryu Jindal
Germann, Timothy Clark

Intended for: 20th Biennial Conference of the APS Topical Group on Shock Compression of Condensed Matter, 2017-07-09 (St. Louis, Missouri, United States)

Issued: 2017-12-12

The Role of Grain Boundary Orientation on Void Nucleation in Tantalum

Eric N. Hahn[1,2 a)], Saryu J. Fensin[1], Timothy C. Germann[2]

[1]*Materials Science and Technology Division, Los Alamos National Laboratory, Los Alamos, NM 94550, USA*
[2]*Theoretical Division, Los Alamos National Laboratory, Los Alamos, NM 94550, USA*
[a)]*Corresponding author: enhahn@lanl.gov*

Abstract. It is generally understood that microstructure plays a significant role in determining the deformation response of materials. During shock compression, grain boundaries serve as dislocation nucleation/pile-up/adsorption sites and grain size can alter the width of the shock front. During tensile release, grain boundaries are often "weak links" where spallation occurs. As such, a current deficit in predictive modeling capability is a quantitative description of these locations and their relative ability to serve as void nucleation sites - a challenging component of such a description is that spallation is inherently stochastic in nature. The inclination of the grain boundary plane with respect to the loading direction is thought to be a critical constituent in the resultant stress and failure at the boundary. Non-equilibrium molecular dynamics simulations are used to statistically quantify the influence of grain boundary inclination on the location of void nucleation and to highlight the emergence of stress hotspots at such boundaries. Boundaries oriented perpendicular to the loading direction are more likely to fail, but grain boundary inclination alone cannot fully predict void nucleation sites.

INTRODUCTION

The dynamic tensile strength of metals is determined by a diverse range of factors including loading history, microstructure, strain rate, and temperature [1–5]. Tensile failure in the high strain-rate regime is termed spallation [6], a process of physical damage evolution beginning from the nucleation of voids (or cracks) that proceeds through growth and coalescence of the void field, which can ultimately result in complete material failure. The void nucleation process is initiated when the local tensile strength of the material is exceeded [6,7]. During spall, more voids can nucleate away from the original nucleation site depending on the rate of relaxation provided by the damage field and rate of tensile loading [8,9]. Several authors have noted that, because spallation is a stochastic process, there is a critical time dependency that manifests in an overdriven stress state which serves as a driving force for nucleation and influences the extent to which damage develops [6,10].

Spall damage and the prevention thereof of interest in many fields due to its pervasiveness in engineering applications. Here, the focus will be on developing a quantitative description of the nucleation process with specific emphasis on a single variable, the inclination of a grain boundary with respect to the loading direction. There have been several recent advances in our understanding of failure in FCC metals such as copper [11–14], but less marked progress in BCC metals. Several papers have evaluated the response of BCC tantalum to shock and spall with a more macroscopic perspective [3,15,16], and, while there are several papers that focus on deformation mechanisms in spalled tantalum [1,17,18], there is still a distinct need to quantify the nucleation process in order to develop predictive capability, especially in polycrystalline samples [15].

METHODOLOGY

Multiple non-equilibrium molecular dynamics simulation methods are available to study spallation of solids [1]. For studying tantalum under shock-like conditions, the Ta1 embedded-atom model potential developed by Ravelo et

al. [20] is highly applicable [21,22]. The present simulations utilize a quasi-isentropic (QI) technique [23] implemented in the Scalable Parallel Short-range Molecular Dynamics (SPaSM) code [24–26]. This methodology allows for homogenous compression and expansion of a fully periodic system at a constant and well-defined strain rate. As such, the QI technique is advantageous when studying spall because failure can occur at any spatial point within the simulation volume, wherever the cohesive strength is weakest or stress hot spots occur. Typical piston or flyer non-equilibrium MD simulations, on the other hand, are implemented such that a small subsection of the total number of grains are subjected to the peak tensile load and the strain rates are very high due to the large system sizes required for shock and rarefaction wave propagation.

The present simulation is 210 nm x 210 nm x 105 nm, containing 253,580,530 atoms and 100 grains created using Voronoi construction. The system is short in the loading direction and larger in the transverse directions to allow for a greater amount of void growth and coalescence, which is expected to favor the directions transverse to the loading direction. Before applying a load, the system is annealed at 2275 K (75% of T_m=3033 K) for 0.5 ns and subsequently cooled to 300 K to allow for relaxation of the grain boundary network. The resulting average grain size is 36 nm, the largest grain is 54 nm, and the grain size distribution is approximately log-normal. The annealing stage allows for grain boundary (GB) curvature resulting in a more realistic microstructure in contrast to the original Voronoi construction with perfectly planar GBs. A comparison of these two states is shown in the upper right hand side of Figure 1; snapshot (1) as-constructed and (2) as-annealed.

The simulation progresses in three stages using 2 fs time steps: QI compression (QIC), NVE "hold", and QI tension (QIT). During QIC the system is taken to -17% true uniaixial strain at a strain rate of 10^9 s^{-1}. True strain is used to allow for ease of restarting the massive simulation over several runs and the uniaxial strain state is chosen to mimic the strain state expected under shock compression. The resultant P_{zz} = 45 GPa is similar to a shock wave in tantalum with U_p ~ 600 m/s. The system is held in this state for 100 ps using an NVE ensemble to allow for the system to equilibrate at this volume, reducing the normal stress and shear stress analogously to the evolution of material located behind a shock front transitioning to a 3D plastic stress state. The material is then unloaded through release and pulled into tension uniaxially at 10^9 s^{-1} - a process comparable to an elastic-plastic shock reflecting from a rear surface and arriving at the spall plane. The simulation is graphically represented in Figure 1 showing several material states and the stress history pathway.

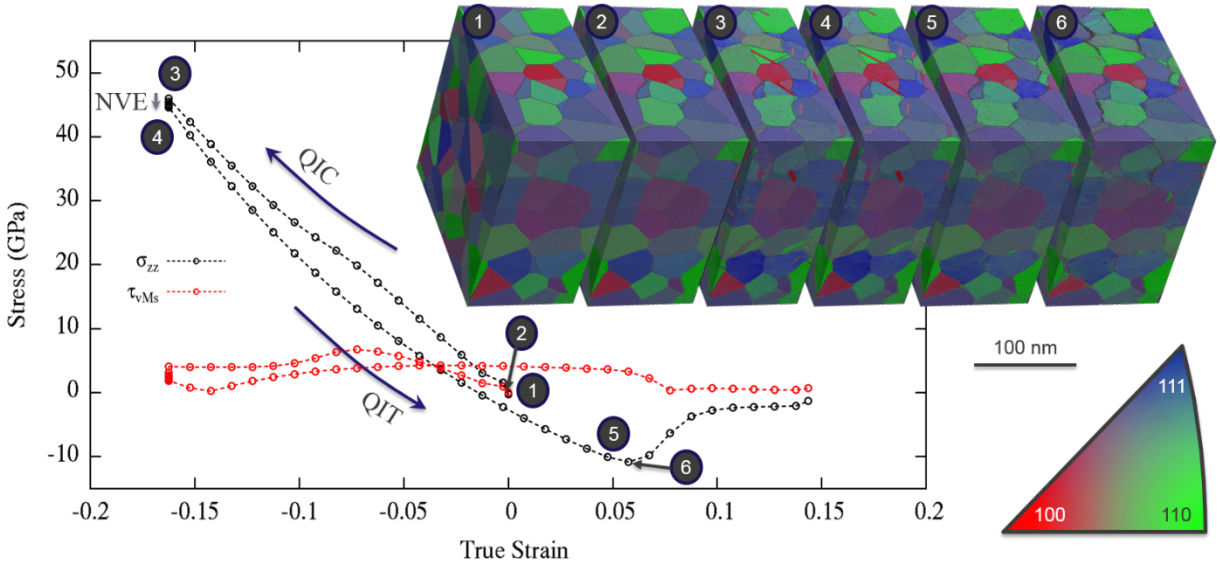

FIGURE 1. Normal stress is given in black and von Mises shear stress in red. System snapshots are given at: (1) initial Voronoi construction; (2) structure following anneal and quench; (3) peak compressive strain following QIC; (4) after NVE hold; (5) first void nucleation during QIT; and (6) peak global tensile stress. The atoms are colored according to a local orientation descriptor where the orientation of the crystal is compared to ideal <001>-red, <011>-green, and <111>-blue orientations and mapped to an RGB color triangle [20]. The sixth state shows free surfaces (void surfaces) colored by gray atoms.

Note that the longitudinal stress (the stress component normal to the loading direction) does not cross through the zero-stress zero-strain condition during QIT. The loading history is critically important when discussing the

spallation response of the material. It is expected that dislocation phenomenon such as the Bauschinger effect will play a role in a complete description, but this (and many other factors) are sidelined for future investigations.

RESULTS

The peak global tensile stress of 11 GPa occurs at 0.064 tensile strain and 1 ns. This value agrees well with previous simulations of 22 nm grain size simulations at a tensile strain rate of 10^9 s^{-1} [1]. The first void nucleates ~0.02 ns earlier at 0.98 ns, 8.4 GPa, and 0.043 tensile strain. Figure 2 shows snapshots at 0.96, 0.98, and 1.0 ns with atoms colored according to their local stress neighborhood. The stress at a given atomic position is taken as the average of the stress of itself and its neighbors (~28) within a 0.53 nm cutoff radius (equivalent to the Ta1 potential cutoff). Figure 2 demonstrates that while the "global" stress value is ~10 GPa, there exist many stress hot spots as well as cold spots.

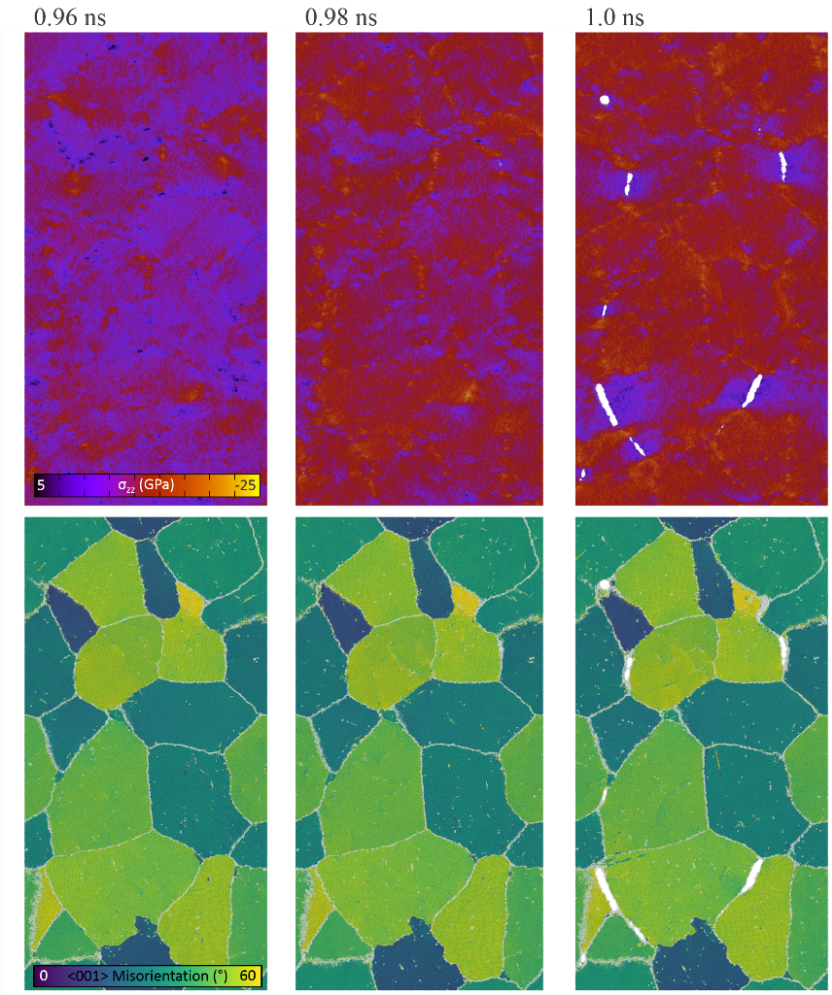

FIGURE 2. Three simulation snapshots with two coloring schemes. The loading direction is horizontal for each Figure in this article. Top row: Evolution of normal stress immediately before and after void nucleation. Bottom Row: Orientation map colored by the misorientation of each crystal from a <001> crystal. Stress hotspots can be seen in the 0.98 ns frame that directly correspond to subsequent void nucleation and growth by 1 ns. In the 1 ns frame, stress relaxation is observed in the vicinity of voids as they open and grow. Several additional hotspots can be seen in the 1 ns frame and depending on the rate of relaxation they may also nucleate voids.

Local normal stress hotspots located at grain boundaries are between 15 and 20 GPa immediately prior to void nucleation, ~1.5x - 2x as high as the global average. It is worth noting that 15 GPa is similar to spall strengths measured for single crystals at this strain rate [1]. It may be posited that grain boundaries are not inherently "weak", but primarily serve as stress concentrators due to compatibility requirements. As the grain size increases, dislocation pileup is expected to play an increased role. The majority of normal stress hot spots occur at boundaries that are aligned perpendicular to the loading direction ($\theta = 90°$). Boundaries aligned with the loading direction ($\theta = 0°$) experience a greater amount of shear stress in agreement with bi-crystal simulations by Fensin et al. [14].

A systematic evaluation of the influence of grain boundary inclination (θ) on void nucleation is performed through serial sectioning. Measurements of the angle between grain boundaries containing a void and the loading direction were taken for 101 voids located in eleven serial slices at 20 nm increments beginning 5 nm away from the periodic y boundary. The selected frame for analysis is 1 ns, coinciding with the peak tensile stress. It is expected that after the stress drop that the system will be firmly in the void growth/coalescence regime. The angle measurements are binned in 5° increments. Symmetric considerations are included, i.e. a boundary at -45° is equivalent to a boundary at 45° and if a boundary has multiple voids it is only counted once. When serial sectioning, the quantity of voids and grain boundaries can be measured in counts or 2D lengths. Both measurements were conducted and give comparable results. For the sake of clarity the data presented here represents probabilities determined from integer counts. Figure 3 displays the results of these measurements as three probabilities. First, in black, the probability of finding a void at a grain boundary of a given orientation, P: $V \cap GB(\theta)$. Second, in red, the probability of finding a grain boundary orientated at a given angle, P: $GB(\theta)$. Third, in blue, the probability of a given boundary orientation exhibiting void nucleation, P: $V \mid GB(\theta)$.

The trend shown in Figure 3 indicates that grain boundaries with planes perpendicular to the loading direction fail preferentially. We see a small peak between 70-75°, possibly indicating that a greater number of grains may need to be sampled. For instance, Fensin et al. [14] measured 700 voids from an experimental specimen binned in 22.5° increments to derive a similar trend for FCC copper. It is also possible that if the analysis was conducted earlier in the simulation, deeper within the nucleation regime, the 70° peak may shift towards 90°.

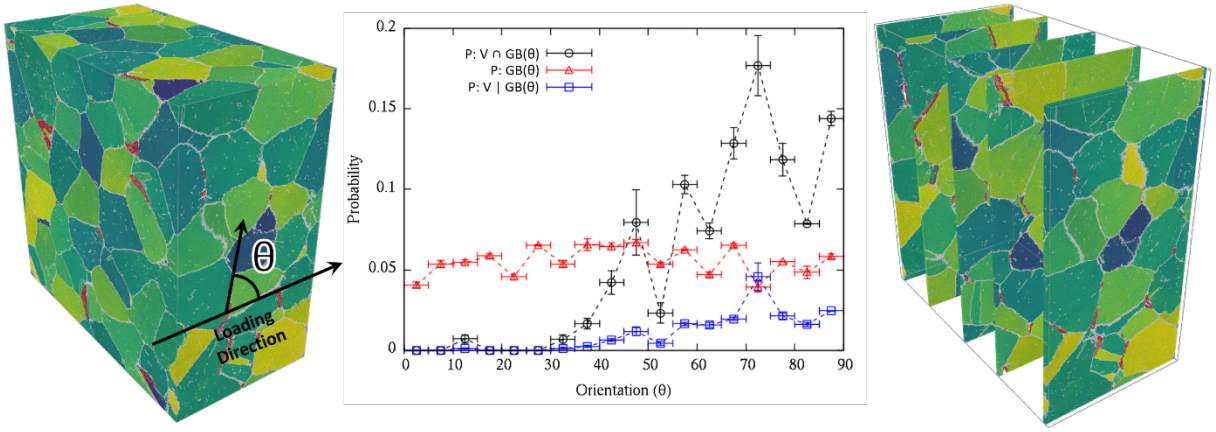

FIGURE 3. Probability of finding various features as a function of grain boundary orientation with respect to the loading direction. Theta is defined as shown in the left figure. Grains are qualitatively colored to aid the eye in distinction. The atoms belonging to void surfaces are colored red and defects are colored white. Five representative slices are shown on the right. The black line with circles gives the probability of finding a void at a grain boundary of a given orientation. The red line with triangles gives the probability of finding a grain boundary at a given orientation. The blue line with squares represents the probability of a given boundary orientation to contain a void.

In order to verify that the trend identified with 2D serial sectioning is representative of a 3D microstructure, a secondary analysis step was conducted for a single section. A slice located 105 nm from the lower y boundary was selected which contains eleven voids. Each GB plane was again measured using a 2D projection. The true 3D GB normal is computed by solving for the plane containing of a triplet of atoms belonging to the grain boundary. The angle, Φ, between the 3D GB normal vector and the loading direction is calculated and converted to θ by $\theta = 90 - \Phi$. Figure 4 displays the section used for analysis and the difference between the 2D and 3D calculations.

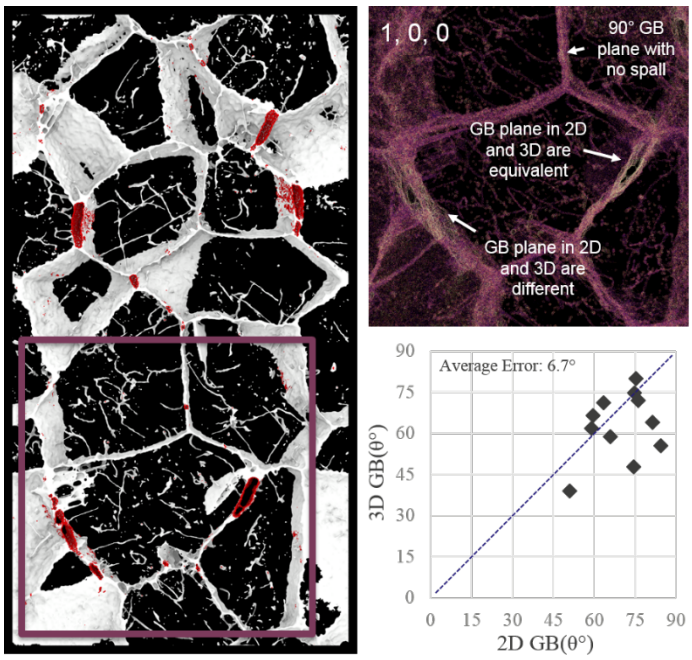

FIGURE 4. Evaluation of 2D and 3D measurements of GB(θ) containing voids. The figure on the left shows a 5 nm slice of the simulation at 1 ns. Grain boundaries are shown as white planes, dislocations as the thin white stings, and void surfaces in red. The figure in the top right shows atoms as a wireframe. Grain boundaries with equivalent 2D and 3D normal vectors are coherent while those with vectors at some angle to one another appear diffuse. The scatter plot on the bottom right shows how the 2D and 3D orientations compare to one another.

Of the eleven GB-void pairs analyzed, six lie below the 1-1 trend, four above, and one on the trend. The average error of 6.7° is larger than a single bin, but on aggregate the analysis shows that a 2D analysis will suffice as positive and negative errors cancel out.

CONCLUSIONS

As a 3D grain boundary surface becomes aligned perpendicular to the loading direction it has a greater cross-sectional commonality with the imposed spall "plane" of maximum tensile stress during dynamic release. The opposite is true for a grain boundary plane aligned parallel with the loading direction. The outcome is that the number of "weak" points sampled is much larger for the perpendicular case as compared to the parallel case. This has a significant influence on the probability to nucleate voids, an inherently stochastic process. Previous work by Fensin et al. [14], related the orientation of the boundary to the resolved normal and shear strains, the former acting more on perpendicular GBs and the later acting more on parallel GBs. A consequence of this is a difference in dilatational strains which are greater in magnitude for perpendicular boundaries and lead to de-cohesion of the boundary. The present work shows that stress hotspots along a given boundary are the primary precursor to void nucleation and that these hotspots more often occur at grain boundaries closer to the perpendicular orientation in agreement with previous analysis. The stress at these hotspots is ~1.5x higher than the bulk stress. It is also shown that the GB orientation trends gathered from serial 2D cross-sections are comparable with trends from 3D analysis, given that the microstructure is not textured and that a sufficient number of voids/GBs are evaluated.

Future work will detail other important properties of a given grain boundary such as its excess energy and volume in addition to the impact of the crystallographic orientations of the neighboring grains and the surrounding GB network. These factors will alter the elastic and plastic response of the boundary by dictating dislocation nucleation, pileup, and transmission across the boundary which are expected to play an important role in spallation. It is evident that within a given grain boundary there are locations more likely to fail. This indicates a sizable contribution of GB heterogeneity which plays an essential role in the void nucleation process.

ACKNOWLEDGMENTS

The MD simulation was run on Trinity (LANL) during Phase 2 of Trinity Open Science. Much appreciation is given to the LANL HPC "Consult" team and especially Louis Vernon. The work was performed as a component of LDRD-2017033DR and numerous useful conversations with Rusty Gray and Curt Bronkhorst are acknowledged. Los Alamos National Laboratory, an affirmative action/equal opportunity employer, is operated by Los Alamos National Security, LLC, for the National Nuclear Security Administration of the U.S. Department of Energy under contract DE-AC52-06NA25396.

REFERENCES

[1] E. Hahn, T. Germann, R. Ravelo, J. Hammerberg, and M. Meyers, Acta Mater. (2016).
[2] S. J. Fensin, S. M. Valone, E. K. Cerreta, and G. T. Gray III, J. Appl. Phys. **112**, 083529 (2012).
[3] G. T. Gray III, N. K. Bourne, V. Livescu, C. P. Trujillo, S. MacDonald, and P. Withers, J. Phys. Conf. Ser. **500**, 112031 (2014).
[4] E. Dekel, S. Eliezer, Z. Henis, E. Moshe, A. Ludmirsky, and I. B. Goldberg, J. Appl. Phys. **84**, 4851 (1998).
[5] M. A. Meyers and C. T. Aimone, Prog. Mater. Sci. **28**, 1 (1983).
[6] T. Antoun, *Spall Fracture* (Springer New York, 2003).
[7] D. R. Curran and L. Seaman, in *High-Press. Shock Compression Solids II* (Springer, New York, NY, 1996), pp. 340–365.
[8] J. Belak, J. Comput.-Aided Mater. Des. **5**, 193 (1998).
[9] S. N. Zhurkov, in *ICF1 Jpn. 1965* (2012).
[10] D. R. Curran, L. Seaman, and D. A. Shockey, Phys. Rep. **147**, 253 (1987).
[11] S. J. Fensin, E. K. Cerreta, G. T. G. Iii, and S. M. Valone, Sci. Rep. **4**, (2014).
[12] S.-N. Luo, T. C. Germann, D. L. Tonks, and Q. An, J. Appl. Phys. **108**, 093526 (2010).
[13] R. W. Minich, J. U. Cazamias, M. Kumar, and A. J. Schwartz, Metall. Mater. Trans. A **35**, 2663 (2004).
[14] S. J. Fensin, J. P. Escobedo-Diaz, C. Brandl, E. K. Cerreta, G. T. Gray III, T. C. Germann, and S. M. Valone, Acta Mater. **64**, 113 (2014).
[15] S. V. Razorenov, G. I. Kanel, G. V. Garkushin, and O. N. Ignatova, Phys. Solid State **54**, 790 (2012).
[16] J. N. Johnson, R. S. Hixson, D. L. Tonks, and A. K. Zurek, AIP Conf. Proc. **370**, 523 (1996).
[17] E. N. Hahn, T. C. Germann, R. J. Ravelo, J. E. Hammerberg, and M. A. Meyers, AIP Conf. Proc. **1793**, 070006 (2017).
[18] A. Strachan, T. Çağın, and W. Goddard, Phys. Rev. B **63**, (2001).
[19] C. Bronkhorst, G. Gray III, F. Addessio, V. Livescu, N. Bourne, S. MacDonald, and P. Withers, J. Appl. Phys. **119**, 085103 (2016).
[20] R. Ravelo, T. C. Germann, O. Guerrero, Q. An, and B. L. Holian, Phys. Rev. B **88**, 134101 (2013).
[21] D. Tramontina, P. Erhart, T. Germann, J. Hawreliak, A. Higginbotham, N. Park, R. Ravelo, A. Stukowski, M. Suggit, Y. Tang, J. Wark, and E. Bringa, High Energy Density Phys. **10**, 9 (2014).
[22] D. R. Tramontina, E. N. Hahn, M. A. Meyers, and E. M. Bringa, AIP Conf. Proc. **1793**, 070002 (2017).
[23] R. Ravelo, B. L. Holian, and T. C. Germann, *High Strain Rates Effects in Quasi-Isentropic Compression of Solids* (Los Alamos National Laboratory (LANL), 2009).
[24] P. S. Lomdahl, D. M. Beazley, P. Tomayo, and N. Gronbech-Jensen, Int. J. Mod. Phys. C **04**, 1075 (1993).
[25] D. M. Beazley and P. S. Lomdahl, in *Proc. 1996 ACMIEEE Conf. Supercomput. 1996* (1996), pp. 50–50.
[26] T. C. Germann and K. Kadau, Int. J. Mod. Phys. C **19**, 1315 (2008).